Langmuir

ARTICLE

pubs.acs.org/Langmuir

Wettability Increase by "Corona" Ionization

Vito Di Virgilio,* Sandra Bermejo, and Luis Castañer

MNT, Department of Electronic Engineering, E.TSE Telecomunicación, Universitat Politècnica de Catalunya, Módul C4 Campus Nord UPC, Jordi Girona 1, Barcelona 08034, Spain

Supporting Information

ABSTRACT: Experiments showing an increase in the wettability of a hydrophobic surface when using corona air ionization are shown. Photoluminiscence observations support the predictions of charge accumulation at the triple line and confirm previous experiments. In all of the experiments, the contact angle was in the saturation regime at a value smaller than that predicted by the condition of a zero value for the solid−liquid surface tension. The PDMS did not show any deterioration due to the corona exposure under the experimental conditions used. The contact angle is shown to increase with humidity.

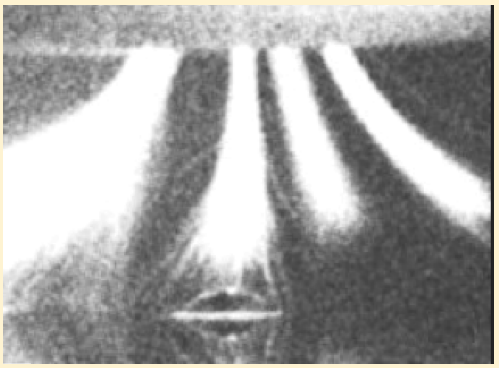

INTRODUCTION

The wettability of a surface has been shown, for many years now, to increase by the application of a voltage difference between the liquid droplet and the substrate,[1−3] which, most often, is a conductor covered by a dielectric (electrowetting on the dielectric, EWOD). There are basically two explanations of the phenomenon. The first one considers that the solid−liquid surface tension is modulated by the electrostatic energy stored by the unit area in the effective capacitance created by the liquid and the substrate.[4] The second explanation considers that there is a net force acting on the electric charge that accumulates at the triple line (TPL) formed among the air, the solid substrate, and the liquid.[5,6] In fact, irrespectively of the explanation given, the contact angle decrease is independent of the polarity of the applied voltage, and the Lippmann−Young[7] equation for the static contact angle change,

$$\cos\theta_V = \cos\theta_0 + \frac{\varepsilon_0\varepsilon_r}{2\gamma_{LV}d}V^2 \qquad (1)$$

has been experimentally demonstrated[8] for a wide range of voltage values prior to a saturation regime.

In eq 1, θ_0 is the contact angle before the voltage is applied, θ_V is the contact angle after a voltage V is applied, ε_0 is the vacuum permittivity, ε_r and d are the relative permittivity and the thickness of the dielectric layer, respectively, and γ_{LV} is the surface tension of the liquid−gas interface. This increase in wettability contrasts with the decrease in wettability observed after electron bombardment.[9]

In a recent paper,[10] we preliminarily discussed a contactless method to increase the wettability by creating the charging conditions of the TPL by air ionization using a corona charge instrument. We are providing in this article a more detailed discussion and systematic measurements of the observations we have made using this technique.

Corona ionizers are based on the ionization of molecules of the surrounding air by the application of a sufficiently high potential between specific geometry electrodes (e.g., pin to plane) creating a large electric field gradient.[11] The control of static charge on insulating materials is a widespread use of this technique in the semiconductor industry to avoid undesired electrostatic discharge (ESD). In fact, this is the only practical way to neutralize static charge because grounding has no effect on the level of charge in insulators.

In this article, we have used corona ionization to build electrostatic charge on a EWOD structure and analyze the effects this may have on the contact angle between a drop and the surface. Our preliminary experiments reported in ref 10 did show that the contact angle decreased after exposure to corona ionization, and this observation motivated the detailed study of the phenomenon that we report here. There are few works relating electrowetting to air ionization. Vallet et al.[12] attributed to air ionization the saturation phenomena of the contact angle, Blake[13] used a corona charging procedure to assist the study of contact angle change for a constant speed moving substrate, and Arifin et al.[14] investigated the effect of the electrohydrodynamic thrust on the movement of particles suspended on a fluid. Moreover, Quinn et al.[8,15] attributed contact angle saturation to the fact that the surface tension between liquid and solid

Received: January 31, 2011

   dx.doi.org/10.1021/la2019583 | *Langmuir* XXXX, XXX, 000–000

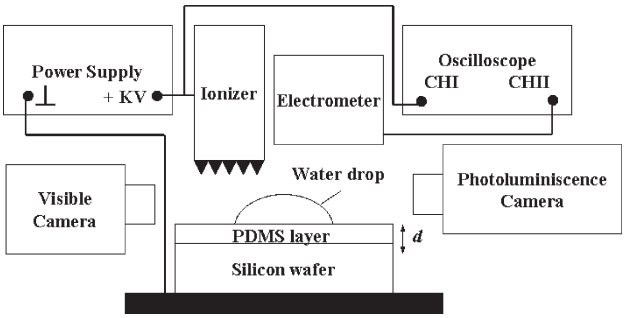

Figure 1. Schematic representation of the measurement setup.

cannot be smaller than zero and hence that the air ionization effect was a concurring effect rather than a limiting one.

In the sections below, we report on several observations that we have made: monitoring of the contact angle change after the corona has been switched on, photoluminescence pictures of the drop and the surrounding area, and surface charge measurements. We show that air ionization has an important effect on the contact angle change, increasing the wettability of the surface. We have then compared the results of these experiments to the results of conventional electrowetting, leading to the conclusion that in the range of experimental voltages explored, the contact angle lies in the saturation regime. We have performed XPS measurements before and after corona exposure to make sure that the observations are not related to the deterioration of the PDMS. Finally, in an effort to contribute to an understanding of contact angle saturation and because the only source of charge in our experiments is the ionization of air, we have made observations of the saturation angle value as the air relative humidity is changed, concluding as shown below that it increases as the RH is increased.

EXPERIMENTAL SECTION

Figure 1 shows the experimental arrangement we have used. It is basically composed of a sample holder placed beneath the corona ionizer, sitting on a metallic plate serving as the bottom electric contact at a controlled distance of 1 cm. The corona ionizer device, commercialized by Simco B.V., provides charges by ionizing the air around five metal needles with a sharp tip of 45 μm radius. The charge is collected and measured by a hand-held electrometer (Electrostatica, S.A.) mounted close by to the corona ionizer, at 1 in. above the substrate. The electrometer generates a TTL-compliant analog signal collected by a digital oscilloscope.

The drop shape is recorded dynamically, and the contact angle is calculated using KSV Cam200 equipment. Photoluminescence is observed using a high-sensitivity camera (Hamamatsu ImagEM) air cooled at −65 °C. The optic is telecentric 1X.

The device tested is basically made by spinning PDMS on a bare silicon wafer. The wafers have first been accurately cleaned in two steps starting with a piranha cleaning and then giving the wafers an HF dip to completely eliminate the thin native oxide from the surface.

PDMS is prepared using the Dow Corning Sylgard 184 kit. To cover a 4 in. wafer, the amount of polymer mixture required is 5 mL of silicone oil mixed with 0.5 mL of curing agent (Sylgard 184, 10:1 ratio). The mixture is then placed in a vacuum chamber in order to purge the bubbles cast in the mixing process.

The wafers have been coated following three different recipes in order to get different thicknesses of PDMS. After an acceleration step of 30 s at 500 rpm, the PDMS has been spun at 500, 1000, and 1500 rpm for 65 s.

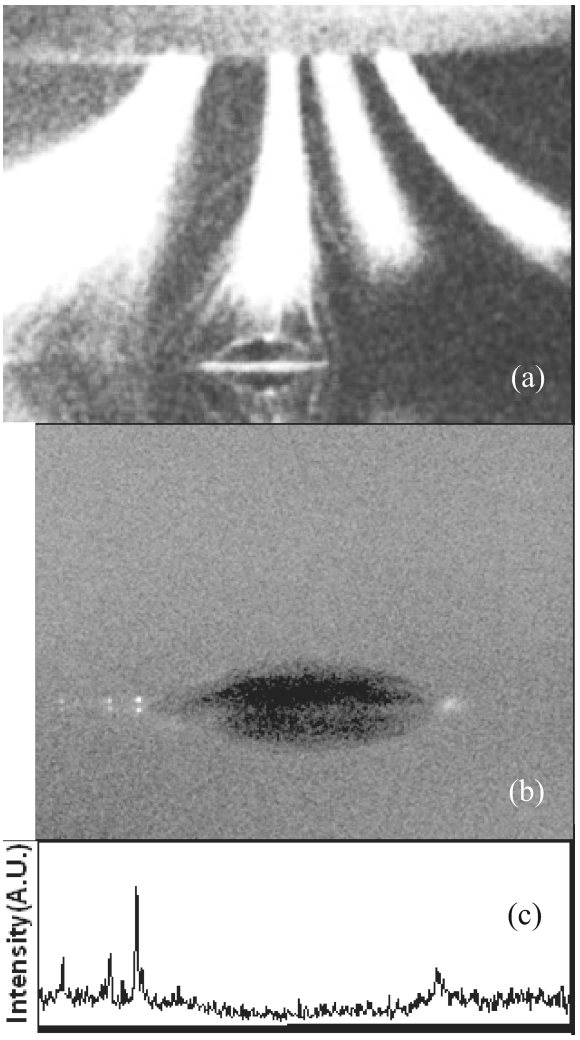

Figure 2. (a) Air breakdown luminescence coming from the five needles of the corona ionizer. Luminescence is also seen on the drop perimeter. (b) Luminescence observed after the high voltage has been switched off. (c) Luminescence intensity, in arbitrary units, on the TPL of the droplet depicted in panel b.

The resulting thicknesses obtained are 69.5, 53, and 44 μm. Once the PDMS was spun, the wafers were dried on top of a hot plate at 70 °C for 30 min.

MEASUREMENT RESULTS

We have carried out systematic measurements using a DI water droplet of 20 μL volume placed at a vertical distance of 1 cm from the corona ionizer head. Once the device was placed in the holder, the power supply was triggered on and hence a high dc voltage (HVDC) was applied to the corona ionizer head. We explored the effects of the value of the HVDC applied, and we did not observe major changes in the contact angle values for the source voltage values below 4 kV, corresponding to the breakdown voltage of air,[16] which is also a function of the humidity.[17] The corona discharge normally appears before brush discharge or sparkover as soon as the electric field reaches a critical value derived by applying the Peek breakdown criterion in a pin-to-plane geometry.[18]

dx.doi.org/10.1021/la2019583 |*Langmuir* XXXX, XXX, 000–000

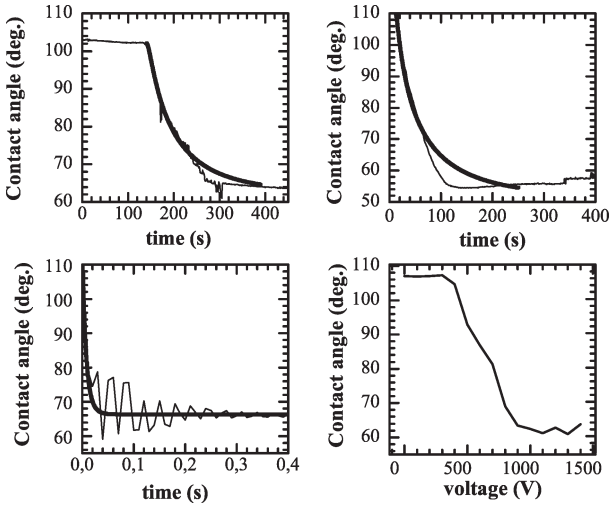

Figure 3. Contact angle as a function of time for several values of the source voltage: 4 kV (upper left), 4.5 kV (upper right), 8 kV (bottom left), and conventional electrowetting (bottom right). All devices had 69.5-μm-thick PDMS, with the exception that at 8 kV the layer was 53 μm thick. The thick lines (upper left, upper right, and bottom left) are model fitting results. All of the measurements were made at a temperature of 20.2−21.4 °C and a humidity of 27−28%.

For our geometry, the corona inception voltage is calculated to be around 2.5 kV of the source voltage, indicating that the inception voltage has to be exceeded in order to notice contact angle changes.

We have made photoluminescence observations with a camera, and a summary of the main results are shown in Figure 2, where the breakdown of air is observed in Figure 2a coming from the corona needles to the drop and the surrounding area. Luminescence coming preferentially from the triple line to the air was observed while the high voltage was still applied (Figure 2b) and also after the high voltage was switched off (Figure 2c). These effects were accompanied by a reduction in the contact angle from initially some 110° to smaller values shown in Figure 2, typically in the range of 55 to 70°, thereby confirming the wettability increase. These observations agree with the observations reported in ref 18, confirming that the charge accumulates at the edge of the drop as was also calculated using the Swartz−Chirstoffel transformation in ref 19 and that the air ionization has effects similar to the direct application of voltage to the drop.

In Figure 3, we show plots of the contact angle measured as a function of time with the help of the CCD camera shown in Figure 1 for several values of the corona ionizer source voltage. This is compared to the results of a conventional electrowetting measurement in the bottom right of Figure 3.

Several things can be concluded from the plots shown in Figure 3. The transient becomes faster as the voltage is increased, as can be seen from the very different time range between the top and bottom left plots. At 4 kV, the transient lasts some time, approximately 150 s, before changes in the contact angle start to be seen. This can be due to the threshold described in ref 15. It can also be seen that higher values of the source voltage produce transients having smaller asymptotic values in the contact angle, although all values are very close to each other between 56 and 64°. Compared to the conventional electrowetting results shown in Figure 3 (bottom right), this indicates that the saturation regime is reached. Finally, we can see in Figure 3 (bottom left) damped oscillations mainly at higher voltages. This is consistent with resonance modes, as described by Oh et al.,[20,21] that predict a resonance frequency of around 20 Hz for the lowest resonance mode, although the model apparently underestimates our observations of resonance frequency typically in the range of 30 Hz.

The modeling of the movement of the fluid as a result of the electrical excitation leads to a free boundary problem between the droplet and the surrounding air or fluid, which has been studied using different approaches for different geometries. The movement of a drop on a surface has been dynamically modeled with the help of a phase-field model.[22] Also, a finite element method for EWOD devices between two parallel plates has been proposed,[23,24] and a shape-inverse approach calculates the curvature.[25] All of these models require CFD tools. More simplifying approaches have been followed by Castañer et al.,[10] neglecting inertia, gravitational effects, and viscous losses or assuming quasi-static conditions for constant triple-line velocity, as in Blake,[13] Berge,[26] and Vallet.[12,27] The conventional molecular kinetic[28] and hydrodynamic[29] models that describe spontaneous wetting could also be applied to model the recovery after excitation[30] but not the transient induced by electrowetting, which is what we are modeling here.

In Figure 3, superimposed on the experimental measurements, fittings to the model described in ref 10 are shown. The model is a lumped model coupling a Thevenin equivalent circuit of the source (V_{th} is the equivalent source voltage and R_{th} is the equivalente resistance) with the simplified differential equations of the dynamic surface tension balance. It should be stressed here that V_{th} and R_{th} model-equivalent circuits of the corona charging setup and hence those two lumped parameters also include practical distributed effects. In the examples shown in Figure 3, the value of R_{th} had to be adjusted to very large values, namely, 4×10^{12} Ω for the 4 kV experiment and 5×10^{12} Ω for the 4.5 kV experiment whereas for a larger voltage, 8 kV, the key parameter for the fitting was the fricition coefficient, which was set to 0.5 Ns/m^2, and the value of R_{th} was irrelevant for $R_{th} < 500$ Ω. We interpret these results from the fact that at higher voltages the supply of charge to the triple line is sufficiently fast that the transient speeed is limited only by friction. At low voltages, however, the transient is limited by the charge supply rate, indicating that the ionization is limited as described in ref 31, and hence we can define a "current-starved" charging supply regime. It also has to be mentioned that the model described in ref 10 did not include saturation effects. The values adjusted from the model for V_{th} provide effective values only for the charge per unit area, $q_{A_{mod}}$, defined as follows:

$$q_{A_{mod}} = \frac{\varepsilon_0 \varepsilon_r}{d} V_{th} \tag{2}$$

In our experiments, the values provided by eq 2 were generally smaller than the measured values of $q_{A_{meas}}$ given by

$$q_{A_{meas}} = \frac{\varepsilon_0 \varepsilon_r}{d} V_{meas} \tag{3}$$

where V_{meas} is the measure of the electrometer. This indicates that we are in the saturation regime.

To confirm this assertion further, we have performed conventional electrowetting with a contact needle in the drop and measure the contact angle as a function of the applied dc voltage. This is shown in Figure 3 (bottom right), where we can see that the saturation angle is around 65°.

dx.doi.org/10.1021/la2019583 |*Langmuir* XXXX, XXX, 000–000

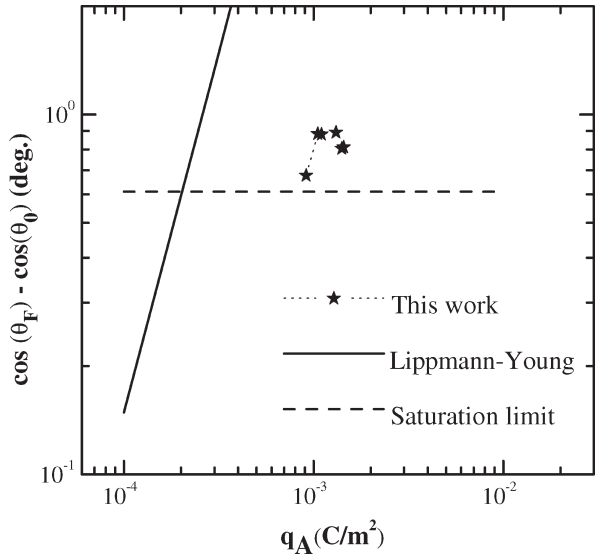

Figure 4. Plot of the values of $(\cos \theta_V - \cos \theta_0)$ as a function of the measured values of the charge per unit area, q_A. Lippmann−Young equation (−), Quinn[15] saturation limit (---), $d = 53\ \mu$m, $\varepsilon_r = 2.62$, $\gamma_{LV} = 72.9 \times 10^{-3}$ N·m, and $\gamma_{SV} = 19 \times 10^{-3}$N·m.

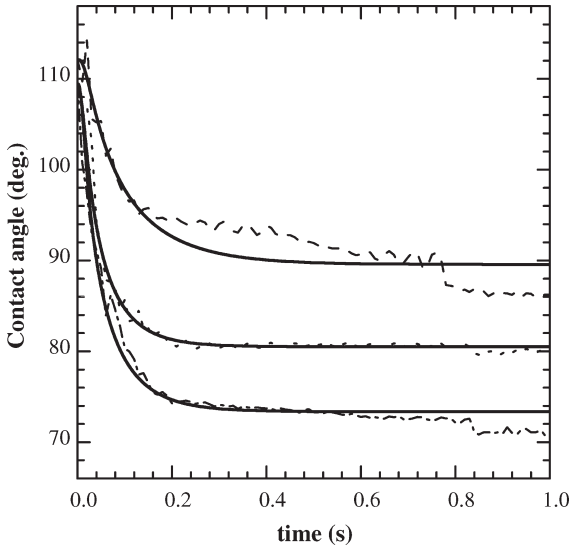

Figure 5. Plots of the contact angle as a function of time for a 7.5 kV source voltage, 69.5-μm-thick PDMS samples, and several values of the relative humidity (46 (−), 60 (···), and 70% (−·−). Solid lines are model fittings. Experiments were carried out at a temperature of 24.4−25.2 °C.

In Figure 4a, plot of $(\cos \theta_V - \cos \theta_0)$ as a function of the charge per unit area, q_A, measured by the electrometer is shown for the 53-μm-thick PDMS samples.

We have also superimposed in Figure 4 the theoretical plot of the Lippmann−Young (−) equation (eq 1) in a log−log plot. Moreover, we have also drawn a horizontal line (---) corresponding to the value given by eq 4,

$$\cos \theta_{SAT} = \frac{\gamma_{SV}}{\gamma_{LV}} \tag{4}$$

which is the contact angle saturation limit predicted by Quinn et al.[8], by stating that the solid−liquid surface tension minimum value is zero. By applying eq 4 to our case, we get $\theta_{SAT} = 74.6°$, and by calculating $(\cos \theta_F - \cos \theta_0)$, we find the value represented in Figure 4 by a horizontal line. All data points in this graph above the horizontal line are beyond the saturation limit predicted by eq 4. In our observations, as shown in the results in Figure 4, the saturation values that we have measured fall beyond the predictions of eq 4.

EFFECTS OF HUMIDITY ON THE CONTACT ANGLE SATURATION

As shown in the section above, in our experiments the saturation regime for the contact angle has been reached and the contact angle saturation value is smaller than the limit predicted by Quinn et al.[8]

This result is consistent with the comparison made in Table 1 in ref 8 of the result of eq 4 with several published experimental results; the agreement was within 13°. (See, for example, the results cited in ref 32.) We have to conclude that apparently eq 4 overestimates the contact angle saturation value. It was also discussed in ref 8 that the interpretation given in Vallet et al.[12] attributing saturation to air ionization was more concurrent that a limiting effect. Recently, additional light has been shed on the saturation effect in liquid−vapor−solid[33] and in liquid−liquid−solid,[30,34] attributing the saturation to trapped charge.[35]

Because in this work we have used air ionization only as source of charge and it is effective in increasing the wettability, it raises the question of whether the humidity in the air can have any effect on the contact angle saturation value. We have carried out some modifications in the experimental setup in order to be able to change the humidity inside a plastic box containing the samples. The relative humidity (RH) was continuously monitored in order to make sure that the RH values did not change during the contact angle dynamics observations.

Figure 5 shows an example of the results that we have obtained.

As can be seen in the main Figure, the contact angle saturates at larger values as the relative humidity increases. It can also be observed that the transient is also slowed down as the RH increases. The change in θ_{SAT} is quite significant because a change in RH from 46 to 70% produces a change in θ_{SAT} from 72 to 86°.

It is difficult to attribute only to eq 4 these changes in the saturation angle because this would require either a smaller value of γ_{SV} or a larger value of γ_{LV} or both simultaneously as the humidity increases. We have not found evidence of such behavior for the surface tensions of PDMS and water in presence of air and variable RH.

Taking into account that the Peek critical field for the breakdown of air increases with humidity and that the corona inception voltage gradient also increases with humidity for a positive corona,[36] our interpretation of the results is that the efficiency of charge transport from the corona area to the interface decreases as the humidity increases, possibly because of the increase in the inception voltage gradient and also the increase in the electrical conductivity of air.[16]

Figure 6 shows a summary of the main results of the humidity effects.

As can be seen, the increase in the contact angle saturation value as the relative humidity increases corresponds to a decrease in the value of model parameter V_{th}, consistent with eqs 1 and 2.

dx.doi.org/10.1021/la2019583 |*Langmuir* XXXX, XXX, 000–000

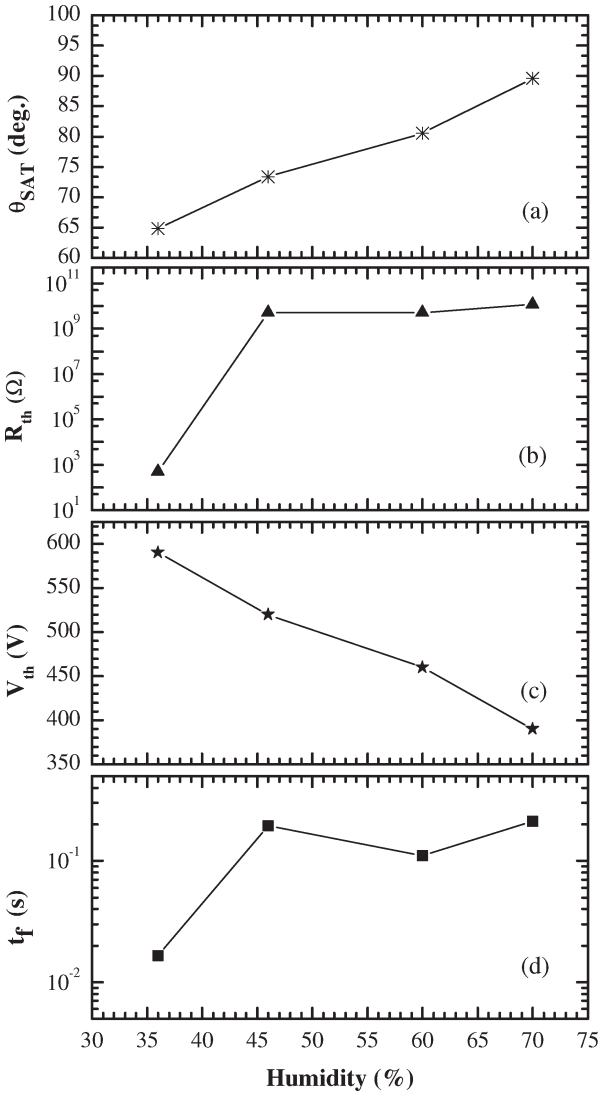

Figure 6. Experimental values of the (a) saturation contact angle value θ_{SAT}. (b) Thevenin equivalent resitance. (c) Thevenin equivalent voltage. (d) Fall time of the contact angle transient from 90 to 10% of the maximum as a function of the relative humidity value.

Moreover, the fall time is seen to increase from low humidity to high humidity values quite sharply as RH gets larger than some 40%, corresponding to a very significant increase (log scale of Figure 6b) in the model parameter R_{th}, thereby indicating that the two parameters are decoupled. These results in Figure 6 support the interpretation that air ionization and air humidity have a significant effect on the transient dynamics of the contact angle and its saturation value.

REVERSIBILITY

In the sections above, we have shown the wettability increase dynamics after corona ionization. In this section, we discuss the reversibility of the effect when the corona ionizer is switched off. A summary of the observations that we have made is the following:

(a) After the drop on top of the PDMS layer has been exposed to the corona and no further manipulation of it is made, the contact angle remains low for a long time (minutes to hours).

(b) If after corona exposure we use a micropipet to suck the drop out and immediately afterwards we deposit a new drop in the same place, then the contact angle recovers totally. (See one of the movies in the Supporting Information section.)

(c) If we first expose the PDMS surface to the corona ionizer for a few seconds with no drop on it and then switch off the corona ionizer and deposit a fresh drop on the surface, then the contact angle is low. If we suck up the drop with a micropipet and deposit a fresh drop in the same place, then the contact angle is fully recovered.

(d) If we expose the PDMS layer to the corona and before depositing a drop on top of it place the sample on top of a hot plate at 40 °C for a few seconds, then the contact angle that we measure after that is the same as before the corona exposure.

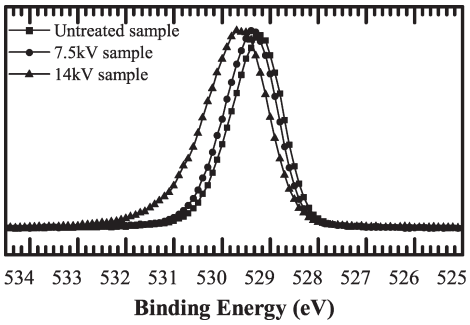

Figure 7. O 1s peaks resolved for the PDMS untreated sample and for corona-treated samples at 7.5 and 14 kV. The untreated and 7.5-kV-treated samples show very similar and symmetric responses whereas the sample treated at 14 kV shows a shift toward higher binding energy and a small asymmetry that can be associated with a different chemical environment.

Before discussing these observations, it is worth reporting on the XPS measurements that we have made on PDMS before and after corona ionization. Let us discuss the possible deterioration of the PDMS due to the corona ionization exposure. It has been reported in the literature that the PDMS surface becomes hydrophilic when exposed to an electrical discharge.[37] It has been described that the main effects of corona discharge on PDMS are the formation of a glassy SiOx surface layer, an increase in the oxygen content of the surface, and the degradation of the network structure.[38] However, PDMS shows the capacity to regain its hydrophobicity after some time. It has been shown that corona exposure with a voltage of 30 kV at a distance of 5 mm for 1 to 30 min creates damage that recovers on a timescale of 100 to 1000 min.[37]

We have investigated the surface damage of PDMS samples by XPS measurements looking into the oxygen contents using a Kratos Ultra DLD system with a nonmonochromatic source (Mg Kα, 1253.6 eV). The measurements have been made at INA (Instituto Universitario de Nanociencia de Aragón, Zaragoza, Spain).

The pressure in the chamber was kept at around 10^{-7} Pa, the sample area is approximately 1 cm^2, and the sampling depth is around 10 nm. The value of the C 1s core of 284.5 eV has been used for the calibration of the energy scale. Three PDMS samples have been cut from the same substrate. One of them was

dx.doi.org/10.1021/la2019583 |*Langmuir* XXXX, XXX, 000–000

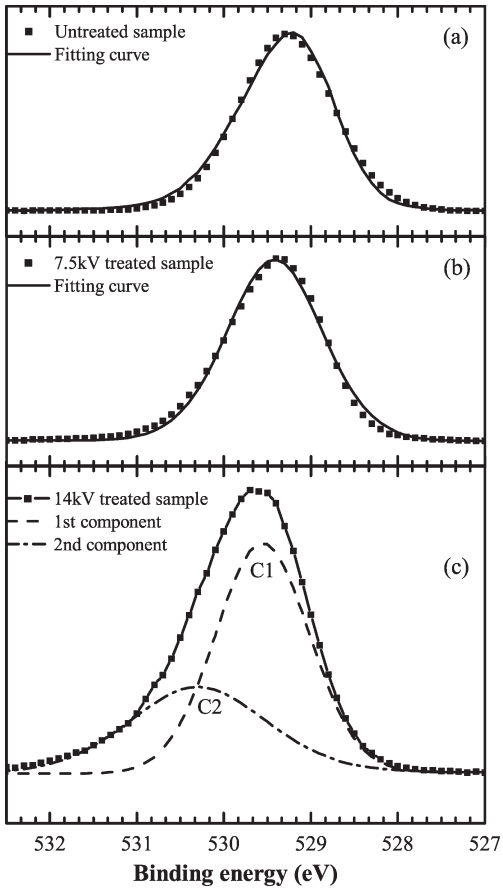

Figure 8. O 1s peaks fitted for (a) the untreated sample and (b) the 7.5-kV- and (c) 14-kV-treated samples. The untreated and 7.5-kV-treated samples show very similar and symmetric responses. They can both be fitted with just one peak, which surely corresponds to unoxidized PDMS. The 14 kV peak shows a small asymmetry that leads to a two-component fitting: C1 at 529.5 eV and C2 at 530.2 eV. Two fitting components mean that oxygen on the surface can be found in two different compounds: unoxidized PDMS, expressed by the peak at lower energy, and partially oxidized PDMS, expressed by the higher-energy peak describing the incorporation of Si−OH groups.

untreated; the others were ionized for 180 s at 7.5 and 14 kV at a controlled distance of 1 cm away from the corona ionizer.

According to ref 39, dc discharge treatment should lead to the incorporation of silanol (Si−OH) groups at the surface of the PDMS whereas the methyl group (CH_3) concentration should decrease.

Figure 7 shows the resolved O 1s peaks. An untreated sample and a 7.5-kV-treated sample show a symmetric and a very similar response with a peak at 529.2 eV for the untreated sample and a peak at 529.4 eV for 7.5-kV-treated sample. These values are in agreement with published data in ref 40. The 14-kV-treated sample exhibits a nonsymmetric peak, shifted toward higher binding energy when compared to the untreated sample and centered at 529.69 eV. The oxidation of the sample surface and the increase in the number of silanol groups (Si−OH) are possibly explained by this peak shift and the asymmetry of this sample analysis. Figure 8a,b depicts the O 1s peaks for the untreated sample and for the treated sample at 7.5 kV, which both can be fitted with just one peak corresponding to unoxidized PDMS. Figure 8c shows the response of the sample treated at 14 kV and fitted with two peaks: the one at lower energy is centered at 529.5 eV and corresponds to O 1s as in unoxidized PDMS, and the second at higher binding energy and centered in 530.2 eV could be associated with the possible incorporation of silanol groups, Si−OH, on the surface. We can conclude that the chemical environment changes when a PDMS sample is submitted to dc ionization on the order of 14 kV whereas it does not if the dc ionization is some 7 to 8 kV for a time of exposure of 180 s.

The reported damage to the PDMS described in refs 37 and 38 was created by a more aggressive electrical discharge than the one that we used in our experiments because the exposure lasted from 1 to 30 min, which is a much longer time than in our case, which was a few seconds, and also the corona voltage was much higher (30 kV compared to a maximum of 14 kV in our case). Finally, the distance between the corona electrode and the drop was in our case twice as long.

In our case, the results shown in Figures 3−5 for the wettability increase were for samples where the experimental conditions were such that XPS measurements did not find material deterioration.

The experiments enumerated in points a−d above are not compatible with PDMS damage recoverable on a timescale of 100 to 1000 min. They are, however, compatible with the effect of mobile charge. Our explanation is that the charge created by the corona ionizer is stored in the capacitance created by the drop, PDMS layer, and substrate and, according to Young's law, reduces the solid−liquid surface tension and decreases the contact angle. If the sample is kept electrically isolated, then the charge remains there for long time and the effect does not revert spontaneously. If some mean is provided for the charge to leave the sample, such as drawing away the drop using a micropipet or by just moderately heating the sample, then the contact angle recovers. The effect of dielectric charging recovery by moderately heating the sample has been extensively used in studies of the dielectric charging of MEMS devices.[41]

CONCLUSIONS

The effects of air ionization on the wettability of hydrophobic surfaces have been investigated by means of a corona ionization instrument and PDMS surfaces on top of a conductive substrate. It has been shown that the wettability increases provided that the corona voltage is above a value that in our case was in the range of 4 kV for our experimental setup. Although in the vicinity of 4 kV the contact angle transients were slower than at higher voltages, the asymptotic value of the contact angle was very similar in all experiments. Model fitting was used to calculate parameter values, and it was concluded that the charge supply to the triple line is the limiting effect for low-voltage values whereas at larger voltages the limiting parameter is the fricition coefficient. We concluded that, in all cases, the asymptotic value of the contact angle was in the saturation regime. The effects of the humidity of the air on the value of the saturation contact angle were also investigated, and a significant increase was observed for increasing values of the relative humidity along with a slowing down of the transient. We conclude that air ionization and the humidity have important effects on the wettability of hydrophobic surfaces and also on the saturation contact angle. Finally, we have provided evidence that the effects observed are not related to the deterioration of the PDMS sample due to electrical discharge.

dx.doi.org/10.1021/la2019583 |*Langmuir* XXXX, XXX, 000–000

■ ASSOCIATED CONTENT

Supporting Information. Two video files. In the first, the corona and breakdown of air are registered using a photoluminescence camera. The luminescence of the triple line can also be seen. The second file shows how the contact angle recovers after the drop is removed from the surface and a new one is deposited. This material is available free of charge via the Internet at http://pubs.acs.org.

■ AUTHOR INFORMATION

Corresponding Author
*E-mail: vito.di.virgilio@upc.edu.

■ ACKNOWLEDGMENT

This work has been supported by MICINN projects TEC-2007-67801 and TEC2010-18222. V.D.V. gratefully acknowledges an FPI grant also provided by MICINN in Spain. Furthermore, we acknowledge the INA (Instituto Universitario de Nanociencias de Aragón, Zaragoza, Spain) for XPS measurements, especially Prof. S. Irusta for her valuable help with the interpolation advice.

■ REFERENCES

(1) Quilliet, C.; Berge, B. *Curr. Opin. Colloid Interface Sci.* **2001**, *6*, 34.
(2) Mugele, F.; Baret, J. C. *J. Phys.: Condens. Matter* **2005**, *17*, R.705–R.774.
(3) Moon, H.; Cho, S. K.; Garrrell, R. L.; Jin, C.; Kim, C. J. *J. Appl. Phys.* **2002**, *92*, 4080.
(4) Zeng, J.; Korsmeyer, T. *Lab Chip* **2004**, *4*, 265–277.
(5) Kang, K. H. *Langmuir* **2002**, *18*, 10318–10322.
(6) Kang, K. H.; Kang, I. S.; Lee, C. M. *Langmuir* **2003**, *19*, 5407–5412.
(7) Lippmann, G. *Ann. Chim. Phys.* **1875**, *5*, 494.
(8) Quinn, A.; Sedev, R.; Ralston, J. *J. Phys. Chem. B* **2005**, *109*, 6268–6275.
(9) Aronov, D.; Molotskii, M.; Rosenman, M. G. *Phys. Rev. B* **2007**, *76*, 035437.
(10) Castañer, L.; Di Virgilio, V.; Bermejo, S. *Langmuir* **2010**, *26*, 16178–16185.
(11) Chua, B.; Wexler, A. S.; Tien, N. C.; Niemeier, D. A.; Holmen, B. A. *J. Microelectromech. Syst.* **2008**, *18*, 115–123.
(12) Vallet, M.; Vallade, M.; Berge, B. *Eur. Phys. J. B* **1999**, *11*, 583–591.
(13) Blake, T. D.; Clarke, A.; Stattersfield, E. H. *Langmuir* **2000**, *16*, 2928–2935.
(14) Arifin, D.; Yeo, L.; Friend, J. *Biomicrofluidics* **2006**, *1*, 01410.
(15) Quinn, A.; Sedev, R.; Ralston, J. *J. Phys. Chem. B* **2003**, *107*, 1163–1169.
(16) Lowke, J. J. *J. Phys. D: Appl. Phys.* **1992**, *25*, 202–210.
(17) Feser, K.; Hughes, R. C. *Electra* **1988**, *117*, 23.
(18) Peek, F. W., Jr. *Dielectric Phenomena in High Voltage Engineering*; McGraw-Hill: New York, 1915.
(19) Schinzinger, R.; Patricio, A. A. L. *Conformal Mapping: Methods and Applications*; Elsevier: Amsterdam, 1991
(20) Oh, J. M.; Ko, S. H.; Kang, K. H. *Phys. Fluids* **2010**, *22*, 032002.
(21) Oh, J. M.; Ko, S. H.; Kang, K. H. *Langmuir* **2008**, *24*, 8379–8386.
(22) Eck, C.; Fontelos, M.; Grün, G.; Klingbeil, F.; O. Vantzos, O. *Interfaces Free Boundaries* **2009**, *11*, 259–290.
(23) Walker, S. W.; Shapiro, B.; Nocheto, R. H. *Phys. Fluids* **2009**, *21*, 102103.
(24) Walker, S. W.; Bonito, A.; Nocheto, R. H. *Interfaces Free Boundaries* **2010**, *12*, 85–119.
(25) Monnier, J.; Witomski, P.; Chow-Wing-Bom; Sheid, C. M. *Siam J. Appl. Math.* **2009**, *69*, 1477–1500.
(26) Berge, B. *C. R. Seances Acad. Sci., Ser. B* **1993**, *317*, 157–163.
(27) Vallet, M.; Berge, B.; Vovelle, L. *Polymer* **1996**, *37*, 2465–2470.
(28) Blake, T. D.; Haynes, J. M. *J. Colloid Interface Sci.* **1969**, *30*, 421.
(29) Voinov, O. V. *Fluid Dyn.* **1976**, *11*, 714–721.
(30) Paneru, M.; Priest, C.; Sedev, R.; Ralston, J. *J. Am. Chem. Soc.* **2010**, *132*, 8301–8308.
(31) Intra, P.; Tippayawong, N. *Chiang Mai J. Sci.* **2009**, *36*, 110–119.
(32) Welters, W. J. J.; Fokkink, L. G. *Langmuir* **1998**, *14*, 1535.
(33) Millefiorini, S.; Tkaczyk, A. H.; Sedev, R.; Efthimiadis, J.; Ralston, J. *J. Am. Chem. Soc.* **2006**, *128*, 3098–3101.
(34) Paneru, M.; Priest, C.; Sedev, R.; Ralston, J. *J. Phys. Chem. C* **2010**, *114*, 8383–8388.
(35) Restolho, J.; Mata, J. L.; Saramago, B. *J. Phys. Chem. C* **2009**, *113*, 9321–9327.
(36) Wang, W.; Li, C.; Luo, B.; Li, X.; Jiang, Y.; An, B.; Wang, Y. *International Conference on Condition Monitoring and Diagnosis*, Beijing, April 21−24, 2008; pp 816−818.
(37) Meincken, M.; Berhane, T. A.; Mallon, P. E. *Polymer* **2005**, *46*, 203–208.
(38) Moreno, V. M.; Gorur, R. S.; Kroese, A. *IEEE Trans. Dielect. Elect. Insul.* **2003**, *10*, 80–95.
(39) Bhattacharya, S.; Datta, A.; Berg, J. M.; Gangopadhyay, S. *J. MEMS* **2005**, *14*, 590–597.
(40) Moulder, J. F.; Stickle, W. F.; Sobol, P. E.; Bomben, K. D. *Handbook of X-ray Photoelectron Spectroscopy*; Perkin-Elmer Corp.: Eden Prairie, MN, 1992.
(41) Molinero, D.; Comulada, R.; Castañer, L. *Appl. Phys. Lett.* **2006**, *89*, 103506.